

Brownian Dynamics of a Sphere Between Parallel Walls

Eric R. Dufresne, David Altman, and David G. Grier

*Dept. of Physics, James Franck Institute, and Institute for Biophysical Dynamics
The University of Chicago, Chicago, IL 60637*

(August 30, 2021)

We describe direct imaging measurements of a colloidal sphere's diffusion between two parallel surfaces. The dynamics of this deceptively simple hydrodynamically coupled system have proved difficult to analyze. Comparison with approximate formulations of a confined sphere's hydrodynamic mobility reveals good agreement with both a leading-order superposition approximation as well as a more general all-images stokeslet analysis.

Stationary surfaces modify the flow field set up by a moving particle, thereby increasing the particle's hydrodynamic drag. Calculating this influence remains a vexing problem in all but the simplest geometries because complicated boundary conditions usually render the problem intractable. For example, Faxén derived a single sphere's hydrodynamic coupling to a rigid planar surface [1] as early as 1924. Adding a second parallel wall, however, is so much more challenging that a definitive formulation is not yet available. This is particularly unsatisfactory in that many biologically and industrially relevant processes are governed by particles' dynamics in confined geometries.

This Letter describes measurements of a single colloidal sphere's diffusion through water in a slit pore formed by two parallel glass surfaces. We use optical tweezers [2] to position the sphere reproducibly within the sample volume, a slow steady Poiseuille flow to establish its position between the walls, and high-resolution digital video microscopy [3] to track its motions in the plane. By positioning a test sphere at selected heights within a slit pore, releasing it and tracking its motions, we are able to measure its height-dependent hydrodynamic coupling to parallel bounding surfaces. These measurements agree quantitatively with predictions based on the stokeslet approximation, a tool which is particularly useful for describing many-body hydrodynamic interactions in colloidal suspensions [4,5].

Previous imaging [6] and light-scattering [7] studies probed confined spheres' dynamics averaged over the slit pore's thickness and only indirectly addressed how a sphere's mobility changes as it moves relative to confining walls. A very recent study combined digital video microscopy with optical tweezer manipulation to measure a sphere's mobility near the midplane of a slit pore as a function of the slit pore's width [8]. Its results cast serious doubt on a recently proposed theory for confined Brownian motion [7], but left open questions regarding a sphere's dynamics at other, less symmetric configurations.

The present measurements were performed on a sin-

gle polystyrene sulfate microsphere from a suspension of spheres $a = 1.006 \pm 0.010 \mu\text{m}$ in radius (Catalog No. 4204A, Duke Scientific) dispersed in an aqueous solution of 2 mM NaCl at $T = 300.66 \pm 0.07^\circ\text{K}$. The sample was cleaned before resuspension by extensive dialysis against deionized water and then infiltrated into a slit pore of area $2 \text{ cm} \times 1 \text{ cm}$ and thickness $H = 8 \mu\text{m}$ created by sealing the edges of a #1 coverslip to a glass microscope slide with uv cured adhesive (Norland Type 88). Access to the sample volume was provided by two glass tubes bonded to holes drilled through the slide at either end of the longest dimension. All glass surfaces were cleaned thoroughly before assembly to ensure uniform surface properties [9]. Although both the sphere and the glass walls develop large surface charges when immersed in water, the suspension's high ionic strength reduced the Debye-Hückel screening length to 7 nm and thus minimized electrostatic interactions. Surface separations were always large enough that van der Waals attractions were negligible [10].

The sample was mounted on the stage of an Olympus IMT-2 inverted optical microscope and imaged with a $100\times$ NA 1.4 oil immersion objective lens. Images captured with an attached CCD camera were recorded on a JVC BRU-S822DXU computer-controlled SVHS video deck before being digitized with a MuTech MV-1350 frame grabber. Computerized analysis [3] of the resulting sequence of digitized images yielded measurements of the colloidal sphere's position in the microscope's focal plane with 20 nm spatial resolution at 1/60 sec intervals [3].

A colloidal sphere diffuses through a Newtonian fluid according to

$$\langle \Delta r_i^2(\tau) \rangle = 2D_i(\vec{r})\tau, \quad (1)$$

where $\Delta r_i(\tau)$ is its displacement in the i -th dimension over time τ and $D_i(\vec{r})$ is the associated diffusion coefficient. Angle brackets indicate an ensemble average. The fluctuation-dissipation theorem relates $D_i(\vec{r})$ to the drag force, $\gamma_i(\vec{r})v_i$, the sphere experiences as it moves past point \vec{r} with speed v_i : $D_i(\vec{r}) = k_B T / \gamma_i(\vec{r})$. The drag

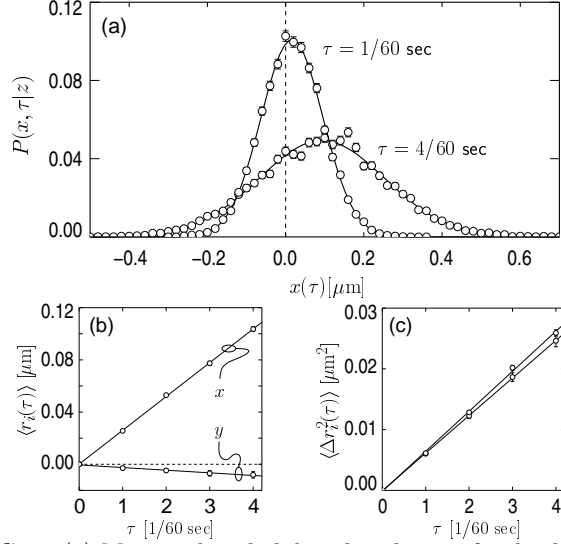


FIG. 1. (a) Measured probability distribution for displacements along the direction of flow at $\tau = 1/60$ sec and $4/60$ sec for $z = 4 \mu\text{m}$. Solid curves are fits to Eq. (3) for the width and displacement of the distribution. (b) Drift of the distributions' centers along and perpendicular to the direction of the imposed flow. (c) Evolution of the mean-square widths of $P(r_i, \tau|z)$, fit to Eq. (1) for $D_i(h)$.

coefficient, γ_i , emerges from the solution to the Stokes equation describing flow at low Reynolds numbers, subject to the surfaces' no-slip boundary conditions.

For example, a sphere of radius a suspended in an unbounded fluid of viscosity η has an isotropic and translation-invariant drag coefficient, $\gamma_0 = 6\pi\eta a$. The corresponding free self-diffusion coefficient for the spheres in the present study is $D_0 = 0.259 \pm 0.04 \mu\text{m}^2/\text{sec}$. A sphere passing between two rigid parallel walls, on the other hand, experiences a drag which depends both on its position z in the slit and also on its direction of motion. Measuring this dependence requires the ability either to track a sphere's motion in three dimensions, or else to position the sphere reproducibly within the slit.

We adopted the second approach, using an optical tweezer to place a single sphere in the microscope's focal plane, releasing it for $t = 5/60$ sec to measure its diffusivity, and then retrapping it. The optical tweezer was formed by directing a collimated beam of laser light (100 mW at 532 nm) through the objective lens' back aperture. Optical gradient forces exerted by the tightly converging beam localized the sphere near the focal point despite radiation pressure and random thermal forces. Suddenly deflecting the beam onto a beam block with a galvanometer-driven mirror extinguished the optical trap and freed the particle to diffuse [5]. Residual heating of roughly 1°C due to steady-state optical absorption relaxed in a few microseconds through thermal diffusion, and did not affect the sphere's dynamics on the time scale

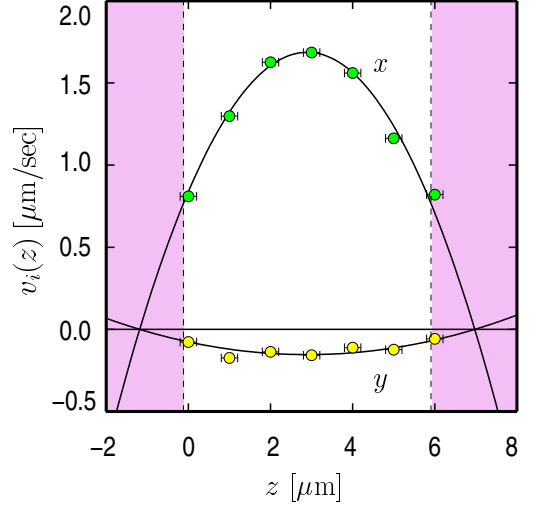


FIG. 2. The drift rate's dependence on initial height in the slit pore. Solid curves result from least squares fits to Eq. (2). Shaded regions are forbidden by sphere-wall contact, given the fit estimates for the wall locations.

of our data collection [3,11]. The galvanometer drive was synchronized to the video camera's sync signal to ensure that data acquisition began at a reproducible interval after the optical trap was extinguished.

We adjusted the focal plane's height in $1.0 \mu\text{m}$ increments to sample the diffusivity's dependence on the sphere's height in the slit pore. The resulting uncertainty in z due to the sphere's out-of-plane diffusion was smaller than $\sqrt{2D_0 t} = 0.2 \mu\text{m}$, and so was small compared with both the sphere's diameter and the separation between walls.

We determined the absolute positions of the glass walls by observing the influence of a steady Poiseuille flow on the particle's motion. The advected sphere attained a height-dependent drift velocity

$$v_i(z) = \frac{4v_{0,i}}{H^2} (z - z_0)(z_0 + H - z). \quad (2)$$

where z_0 is the position of the lower wall. This drift caused the probability distribution for finding the sphere at position \vec{r} to shift as it broadened with time:

$$P(r_i, \tau|z) = \sqrt{\frac{1}{2\pi\langle\Delta r_i^2(\tau)\rangle}} \exp\left(-\frac{[r_i - \langle r_i(\tau)\rangle]^2}{2\langle\Delta r_i^2(\tau)\rangle}\right), \quad (3)$$

where $\langle r_i(\tau) \rangle = v_i(z)\tau$ is the mean displacement in the i -th direction after time τ given the steady flow in that direction at height z .

At each tweezer height z , we collected 3,000 sequences of 5 video fields, yielding 12,000 measurements of $P(x, \tau|z)$ and $P(y, \tau|z)$ over four $1/60$ second intervals. Typical examples at the midplane of the slit pore appear in Fig. 1(a). The peaks' drifts, plotted in Fig. 1(b), yield

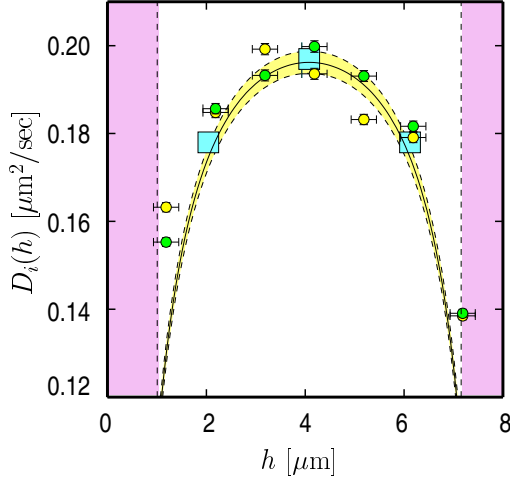


FIG. 3. Height dependence of the in-plane diffusion coefficient for a Brownian sphere in a slit pore. The solid curve results from the Stokeslet approximation and is indistinguishable from the linear superposition approximation's prediction. Dashed curves show the range of predicted values due to the uncertainty in the sphere's radius. Squares show Faxén's predictions from Eq. (6).

components of the drift velocity, $v_i(z)$, which appear in Fig. 2. Fitting $v_i(z)$ to Eq. (2) for $v_{0,i}$, H , and z_0 , yields $H = 8.16 \pm 0.22 \mu\text{m}$ and fixes the lower wall's absolute position to within $\pm 0.13 \mu\text{m}$. Errors primarily reflect the experimental uncertainty of $\pm 0.25 \mu\text{m}$ in the increment between tweezer locations. Without loss of generality, we set $z_0 = 0$ and measure starting heights $h = z - z_0$ from the lower glass surface.

The evolution of the distributions' widths over time, shown in Fig. 1(c), can be interpreted with Eq. (1) to obtain the drag-corrected self-diffusion coefficients $D_i(h)$ for each height. Results are summarized in Fig. 3. As expected, the in-plane diffusion coefficients measured for motions along and transverse to the imposed flow agree to within 5% at all heights. The sphere's diffusivity is strongly suppressed near either wall, and falls well below D_0 even along the midplane.

Faxén's result for the drag on a sphere near a single wall provides a good starting point for interpreting these observations. His result for the in-plane drag, $\gamma_1(h)$,

$$\frac{\gamma_0}{\gamma_1(h)} = 1 - \frac{9}{16} \frac{a}{h} + \mathcal{O}\left(\frac{a^3}{h^3}\right) \quad (4)$$

has been verified to great accuracy using photonic force microscopy in a thick sample cell [12]. Oseen suggested in 1927 that the drag due to two parallel walls could be approximated by a sum of two such single-wall contributions [13]:

$$\gamma_2(h) \approx \gamma_0 + [\gamma_1(h) - \gamma_0] + [\gamma_1(H - h) - \gamma_0]. \quad (5)$$

Even though this linear superposition approximation violates boundary conditions at both bounding surfaces, the corresponding prediction for the in-plane diffusivity, $D_2(h) = k_B T / \gamma_2(h)$, agrees quite well with our measurements, with no adjustable parameters, as can be seen in Fig. 3. Higher-order corrections [1] to $\gamma_1(h)$ yield negligibly small corrections to $D_2(h)$ and so are not presented.

Faucheux and Libchaber adopted the linear superposition approximation, averaged the resulting in-plane diffusivity over h , and obtained reasonably good agreement with h -averaged measurements for various sphere radii [6]. Lin, Yu and Rice further demonstrated linear superposition's accuracy at $h = H/2$ by measuring a sphere's in-plane and out-of-plane diffusivity near the midplanes of slit pores of various widths [8].

Regardless of its empirical success, the linear superposition approximation fails to satisfy boundary conditions and so cannot yield accurate predictions under all circumstances. Lobry and Ostrowsky attempted to remedy its shortcomings by accounting for flows' reflections off bounding surfaces [7]. Considering such corrections up to third order, they obtained results which compare rather poorly with measurements by Lin, Yu and Rice [8].

Faxén managed to calculate two-wall drag coefficients for the particularly symmetric arrangements $h = H/4$ and $h = H/2$ [1]. The in-plane results,

$$\frac{\gamma_0}{\gamma_F(h)} = \begin{cases} 1 - 0.6526 \frac{a}{h} + 0.1475 \frac{a^3}{h^3} - 0.131 \frac{a^4}{h^4} - 0.0644 \frac{a^5}{h^5}, & h = \frac{H}{4} \\ 1 - 1.004 \frac{a}{h} + 0.418 \frac{a^3}{h^3} + 0.21 \frac{a^4}{h^4} - 0.169 \frac{a^5}{h^5}, & h = \frac{H}{2} \end{cases} \quad (6)$$

appear as squares in Fig. 3 and agree well with both Oseen's approximation and also with our measurements. Unfortunately, Faxén's method does not work for other configurations.

Another approach, due to Blake [14], takes advantage of an analogy between hydrodynamics and electrostatics. Rather than attempting to satisfy no-slip boundary conditions at a bounding wall directly, Blake introduced the notion of a hydrodynamic image whose flow field exactly cancels the particle's on the boundary. Uniqueness of the Stokes equation's solutions guarantees that the image solution also solves the original problem.

Blake's treatment yields the Green's function for a particle's flow field bounded by a single surface. Accounting for a second parallel surface involves adding not only the particle's hydrodynamic image in the new surface, but also an infinite series of images of the images. Liron and Mochon [15] summed this series explicitly for a point force acting on the confined fluid, derived the additional terms needed to cancel residual flows on the surfaces, and thereby obtained the Green's function, $G(h\hat{z} - \vec{r}, H)$, for the flow at \vec{r} due to a disturbance a height h above the lower wall in a slit pore of width H . Integrating their

result over the sphere's surface would yield an accurate though unwieldy expression for $\gamma(h)$.

A much simpler solution can be obtained when far field contributions dominate the flows at the bounding surfaces. This is the case when the sphere is much smaller than the gap between the walls, $a \ll H$. In this limit, the flow field due to the sphere's hydrodynamic images is well approximated by the image flow for a point force. Thus, the drag on a sphere centered a height h above the lower wall may be approximated by

$$\gamma^{-1}(h) \approx \gamma_0^{-1} + [G(0, H) - G_S(0)], \quad (7)$$

where $G_S(0)$ is the singular contribution due to a unit point force at the sphere's location, so that the term in square brackets is the flow at the sphere's location due to the images alone. More generally, $G_S(\vec{r})$ is the Green's function in an unbounded fluid and is known as a stokeslet. Eq. (7), then, is an example of a stokeslet approximation. Evaluating Eq. (7) using the expressions for $G(\vec{r})$ and $G_S(\vec{r})$ in Equations (5), (15), (32) and (33) of Ref. [15] yields the in-plane diffusion coefficient

$$\frac{D(h)}{D_0} = 1 + \frac{3}{4} \frac{a}{H} \int_0^\infty \left[A_0 \left(\lambda, \frac{h}{H} \right) - \lambda^2 A_1 \left(\lambda, \frac{h}{H} \right) - 1 \right] d\lambda, \quad (8)$$

where

$$A_0(\lambda, \eta) = 2 \frac{\sinh(\lambda\eta) \sinh[\lambda(1-\eta)]}{\sinh(\lambda)} \quad (9)$$

is the contribution due to a stokeslet at the sphere's position together with an infinite series of image stokeslets, and

$$A_1(\lambda, \eta) = \frac{1}{\sinh^2(\lambda) - \lambda^2} \times \left\{ \eta^2 \sinh(\lambda) \cosh[\lambda(1-2\eta)] - \sinh(2\lambda\eta) + \lambda\eta^2 \sinh^2[\lambda(1-\eta)] + \coth(\lambda) \sinh^2(\lambda\eta) - \frac{\lambda}{4} \left[\frac{(2-\eta) \sinh(\lambda\eta) - \eta \sinh[\lambda(2-\eta)]}{\sinh(\lambda)} \right]^2 \right\} \quad (10)$$

enforces the no-flow boundary conditions at the walls. The numerically evaluated result appears as the solid curve in Fig. 3.

Remarkably, the predictions of Eqs. (8), (9) and (10) are indistinguishable from Oseen's superposition approximation for our experimental conditions, and both agree quantitatively with Faxén's fifth-order results, Eq. (6). Further comparison with Eq. (6) reveals that the stokeslet approximation becomes increasingly accurate for larger wall separations, while the linear superposition approximation fares less well. For smaller separations, on

the other hand, the stokeslet approximation becomes less accurate. Linear superposition performs surprisingly well at small separations, by contrast, particularly if higher order corrections to Eq. (4) are included.

Despite the apparent complexity of Eqs. (8), (9) and (10) when compared with the linear superposition approximation, stokeslet analysis has the appeal of scalability. Under conditions for which the stokeslet approximation is valid, contributions to the diffusivity tensor for a system of spheres can be combined in a straightforward manner [4], as in Eq. (7). We recently demonstrated this approach's utility in the comparatively simple case of two spheres near one wall for which linear superposition yields inaccurate predictions [5]. Further demonstrating its accuracy for the much more challenging case of two-wall confinement lends confidence in its potential for systematically treating many-body colloidal hydrodynamics.

We are grateful to Todd Squires and Michael Brenner for introducing us to stokeslet analysis in general and to Ref. [15] in particular. This research was supported primarily by the National Science Foundation through Award Number DMR-978031. DA was supported in part by The University of Chicago MRSEC REU Program through Award Number DMR-980595. Additional support was provided by the David and Lucile Packard Foundation.

-
- [1] J. Happel and H. Brenner, *Low Reynolds Number Hydrodynamics* (Kluwer, Dordrecht, 1991).
 - [2] D. G. Grier, *Cur. Opin. Colloid Int. Sci.* **2**, 264 (1997).
 - [3] J. C. Crocker and D. G. Grier, *J. Colloid Int. Sci.* **179**, 298 (1996).
 - [4] M. P. Brenner, *Phys. Fluids* **11**, 754 (1999).
 - [5] E. R. Dufresne, T. M. Squires, M. P. Brenner, and D. G. Grier, in press (2000).
 - [6] L. P. Fauchaux and A. J. Libchaber, *Phys. Rev. E* **49**, 5158 (1994).
 - [7] L. Lobry and N. Ostrowsky, *Phys. Rev. B* **53**, 12050 (1996).
 - [8] B. Lin, J. Yu, and S. A. Rice, *Phys. Rev. E*, in press (2000).
 - [9] M. L. Hair, in *Clean Surfaces*, edited by G. Goldfinger (Marcel Dekker, New York, 1970), pp. 269–284.
 - [10] B. A. Pailthorpe and W. B. Russel, *J. Colloid Int. Sci.* **89**, 563 (1982).
 - [11] J. C. Crocker and D. G. Grier, *Phys. Rev. Lett.* **73**, 352 (1994).
 - [12] A. Pralle, E.-L. Florin, E. H. K. Stelzer, and J. K. H. Hörber, *Appl. Phys. A* **66**, S71 (1998).
 - [13] C. W. Oseen, *Neuere Methoden und Ergebnisse in der Hydrodynamik* (Akademische Verlagsgesellschaft, Leipzig, 1927).
 - [14] J. R. Blake, *Prog. Colloid Polymer Sci.* **70**, 303 (1971).
 - [15] N. Liron and S. Mochon, *J. Eng. Math.* **10**, 287 (1976).